# Stable stratification effects on the flow past surface obstructions: A numerical study

**D. A. Trifonopoulos and G. C. Bergeles**
Laboratory of Aerodynamics, Department of Mechanical Engineering, National Technical University of Athens, Athens, Greece

Numerical predictions of the stably stratified flow fields past surface-mounted obstructions are presented. The time-averaged Reynolds equations, coupled with the continuity and temperature/concentration equation for the incompressible fluid, have been solved in the transformed space, using finite differences, adopting the Boussinesq approximation to account for density variations. Buoyancy effects on turbulence have been considered in the two-equation k-ε model, which has been used as a turbulence closure. The turbulent flow fields over a two-dimensional fence and around a three-dimensional hill were simulated for neutral and various stable conditions. The decrease of the cavity wake length behind the two-dimensional fence, due to the temperature gradient, was clearly depicted by the computations. The stability effects on the mean flow past the three-dimensional axisymmetric hill, for various Froude numbers, were reproduced satisfactorily, although some underestimation of the buoyancy influences in some cases was observed. The boundary layer lee side separation was suppressed with increasing stability, and the beginning of a hydraulic jump was predicted for Froude numbers smaller than unit. The comparison between the computations and the available measurements established the reliability of the presented method.

**Keywords**: stable stratification; flow over three-dimensional hill; finite differences; turbulence modeling; Boussinesq approximation

## Introduction

Stratification plays a dominant role in the flow development and the effective dispersion of pollutants over complex terrain. A number of studies, both experimental and theoretical, have shed light onto the stably stratified flow fields past two-dimensional (2-D) and three-dimensional (3-D) obstacles. Brighton (1978) described the structure of the strongly stratified flow past a 3-D hill; he observed that for low Froude numbers the flow field could be subdivided into four different levels. At the two lowest levels the fluid goes round the hill sides, moving at almost horizontal planes. In the third level (near the hill summit) the fluid passes over the top of the hill and lee waves are formed further downstream. In the fourth layer, which lies above the hill, the fluid is slightly affected by the presence of the obstacle. Hunt and Snyder (1980) conducted experiments on stably and neutrally stratified flows over a 3-D model hill. Their neutral flow experiments were conducted in a wind tunnel while the stably stratified studies were made in a towing tank. For Froude numbers of the order of unity they classified the lee-wave patterns and the recirculating regions. For Froude numbers lower than unity they suggested that streamlines pass over the hill top only if they originate at a hill height $H_d$ greater than $h(1 - \mathrm{Fr})$, with $h$ the hill height and Fr the Froude number. The dividing streamline concept mentioned above was further and more analytically discussed and proved successful by Snyder *et al.* (1985) in experiments with models of a 3-D hill, triangular and sinusoidal ridges, and fences and 2-D ridges. Castro *et al.* (1983) studied experimentally the stratified flow field structure over 3-D ridges; their results were consistent with the dividing streamline concept. Rowe *et al.* (1981) made field studies of stable air flow around a ridge, and they found that the obtained data were consistent with a simple two-layer model based on the dividing streamline concept. Hunt (1980) developed a linear theory by combining inviscid potential flow and existing observations to give an extensive description of the flow fields over 2-D and 3-D hills for various classes of stability. Thompson *et al.* (1988) compared observed streamline trajectories with the ones resulting from the application of the linear theory for several stable cases; discrepancies especially with increasing stability were observed, showing the inability of the linear theory to simulate stable flows adequately. Several numerical studies on flow over surface-mounted obstacles have been published. Bergeles and Athanassiadis (1982) presented predictions of the 2-D flow field over a square prism using the k-ε turbulence model, and their results simulated satisfactorily the features of the downstream bubble. Benodekar *et al.* (1985) presented numerical predictions of the neutral turbulent flow over surface-mounted ribs, employing the k-ε model of turbulence in the two dimensions; their predictions for the flow over a square rib and a thin one compare well with the experiments, and the observed discrepancies are attributed to the turbulence modeling. Also Mouzakis and Bergeles (1991) predicted accurately the neutral flow over a 2-D ridge. Haussling (1977) presented a numerical solution of the time-dependent 2-D Navier-Stokes equations for the stable flow over barriers. For low Richardson numbers (i.e., weak stratification) the streamlines over the barrier were found to be about the same with those for the neutral case, but with increasing stratification the downstream cavity was decreased,

Address reprint requests to Dr. Bergeles at the Department of Mechanical Engineering, National Technical University of Athens, 42 Patission St., 10682 Athens, Greece

Received 28 May 1991; accepted 14 November 1991

while the upstream one was significantly increased. Also vortices were formed after the barrier at some distance from it. The numerical work of Haussling depicted interesting phenomena, but no comparison with experimental observations was made.

In the present paper a numerical method for studying stably stratified flow fields is presented. The reliability of the method is established by comparing predictions with available experimental data. Neutral flow fields are also simulated for reference purposes. The method employs the time-averaged Reynolds equations for the incompressible fluid, together with the continuity and temperature/concentration equation. Turbulence is accounted for using the two-equation k-$\varepsilon$ model. Buoyancy effects are included in the k and $\varepsilon$ transport equations. The equations are solved in the transformed space, where difficulties encountered by other methods in the correct representation of the geometry of the complex domain, and the accurate imposition of the boundary conditions, are alleviated. The reliability of the method has been established in previous work for neutral environmental flows (Glekas *et al.*, 1987; Trifonopoulos *et al.*, 1989). The present work is an extension of the method of stably stratified flow fields.

In the next paragraphs the mathematical formulation of the problem, associated physical hypotheses, and numerical solution of the equations are presented, followed by the detailed presentation and discussion of the results of the studied flows. Finally, conclusions on the reliability of the method to investigate stable flows over a broad range of Froude numbers are drawn.

## Mathematical formulation

### *The governing equations*

The cases considered in this paper deal with the steady state flow problem. The fluid is viscous and incompressible, and the density stratification is attributed to the temperature or salinity concentration differences. The Boussinesq approximation is adopted to account for density stratification, so that density variations appear only in the gravity terms. The equations describing the turbulent stratified flow written in Cartesian tensorial form are the following.

Continuity equation:

$$\frac{\partial(\rho u_i)}{\partial x_i} = 0, \quad (i = 1, 2, 3) \tag{1}$$

## Notation

| | |
|---|---|
| $A_i$ ($i$ = E, W, N, S, D, U) | Coefficients in finite difference equations linking the adjacent grid nodes |
| $c_1$, $c_2$, $c_{3\varepsilon}$, $c_\mu$ | Constants of the turbulence model |
| $D$ | The depth of the towing tank |
| Fr | The densimetric Froude number |
| $g$ | The gravity acceleration |
| $G$ | The destruction of turbulence due to buoyant forces, $G = -g/T\overline{u_2'T'}$ |
| $H$ | The fence height |
| $h$ | The axisymmetric hill height |
| J | The Jacobian of the coordinate transformation |
| k | The turbulent kinetic energy |
| $l$ | The mixing length |
| $P$ | The generation of turbulence due to shear, $P = -\overline{u_2'u_1'}\frac{\partial u_1}{\partial y} - \overline{u_2'u_3'}\frac{\partial u_3}{\partial y}$ |
| $p$ | Static pressure |
| $R_f$ | The flux Richardson number, $R_f = G/P$ |
| $R_f'$ | Modified flux Richardson number, $R_f' = G/(P+G)$ |
| $R_i$ | The gradient Richardson number, $R_i = \frac{g}{T}\frac{\partial T}{\partial y}\left[\left(\frac{\partial u_1}{\partial y}\right)^2 + \left(\frac{\partial u_3}{\partial y}\right)^2\right]$ |
| $R_L$ | The cavity wake length |
| $T$ | Temperature/salinity concentration |
| $T_a$ | The ambient air temperature in the wind tunnel |
| $T_f$ | The temperature of the wind tunnel floor |
| $U$ | The free stream velocity |
| $U_t$ | The towing speed |
| $u_i$ | The Cartesian velocity components |
| $X_i$ | The transformed space coordinates |
| $x_i$ | The physical space coordinates |
| $x_{sep}$ | The downwind distance of the separation point from the hill top |
| $y$ | The direction normal to the ground |
| $y_p$ | Distance of the first grid point from the wall |
| $y^+$ | Normalized distance from the wall, $y^+ = \rho c_\mu^{0.25} k^{0.5} y_p/\mu$ |

*Greek symbols*

| | |
|---|---|
| $\beta$ | Volumetric expansion coefficient of the fluid |
| $\delta_{ij}$ | The Kronecker delta |
| $\delta$ | The boundary-layer thickness |
| $\varepsilon$ | The turbulent energy dissipation rate |
| $\mu$ | The dynamic viscosity of the fluid |
| $\mu_t$ | The turbulent viscosity |
| $\rho$ | The fluid density |
| $\rho_r$ | The reference density |
| $\sigma_\varepsilon$ | The turbulent Prandtl number for the dissipation rate $\varepsilon$ |
| $\sigma_k$ | The turbulent Prandtl number for the turbulent kinetic energy k |
| $\sigma_T$ | The turbulent Prandtl number for the temperature/concentration |
| $\phi$ | Dependent variable in finite difference equations |

Momentum equation:

$$\frac{\partial(\rho u_j u_i)}{\partial x_j} = -\frac{\partial p}{\partial x_i} + \frac{\partial}{\partial x_j}\left[\mu\left(\frac{\partial u_i}{\partial x_j} + \frac{\partial u_j}{\partial x_i}\right) - \rho\overline{u_i' u_j'}\right] + g_i(\rho - \rho_r), \quad i,j = 1,2,3 \quad (2)$$

where $g_i$ is the gravity acceleration component along the $i$-direction and $\rho_r$ is the reference density.

Temperature/concentration equation:

$$\frac{\partial(\rho u_i T)}{\partial x_i} = \frac{\partial}{\partial x_i}\left(\frac{\mu}{\sigma_T}\frac{\partial T}{\partial x_i} - \overline{\rho u_i' T'}\right), \quad i = 1,2,3 \quad (3)$$

with $\sigma_T$ as the turbulent Prandtl number for temperature or salinity concentration. Although there is a buoyancy influence on the turbulent Prandtl number (Rodi, 1980), in the present work, $\sigma_T$ was taken constant and equal to 0.9, a value that has given successful predictions in previous numerical studies of buoyant flows (Ince and Launder, 1989).

In order for the above equations to become a closed set, a turbulence closure is needed. The two-equation k-ε model of Launder and Spalding (1974) is used to model the turbulent shear stresses $-\rho\overline{u_i' u_j'}$. The shear stresses are written as

$$-\rho\overline{u_i' u_j'} = \mu_t\left(\frac{\partial u_i}{\partial x_j} + \frac{\partial u_j}{\partial x_i}\right) - \tfrac{2}{3}\delta_{ij}\rho k, \quad i,j = 1,2,3 \quad (4)$$

where k is the turbulent kinetic energy defined as $2k = \overline{u_i' u_i'}$, $\delta_{ij}$ is the Kronecker delta, and $\mu_t$ is the turbulent viscosity expressed as $\mu_t = \rho c_\mu k^2/\varepsilon$, where $\varepsilon$ is the turbulent kinetic energy dissipation rate and $c_\mu$ is a model constant taken equal to $c_\mu = 0.09$.

The velocity temperature fluctuations correlations, $\overline{\rho u_i' T'}$, are also modeled as follows:

$$-\overline{\rho u_i' T'} = \frac{\mu_t}{\sigma_T}\frac{\partial T}{\partial x_i}, \quad i = 1,2,3 \quad (5)$$

The transport equations for the turbulent kinetic energy k and its dissipation rate ε are expressed as

$$\frac{\partial(\rho u_i k)}{\partial x_i} = \frac{\partial}{\partial x_i}\left(\frac{\mu_t}{\sigma_k}\frac{\partial k}{\partial x_i}\right) + P + G - \rho\varepsilon, \quad i = 1,2,3 \quad (6)$$

$$\frac{\partial(\rho u_i \varepsilon)}{\partial x_i} = \frac{\partial}{\partial x_i}\left(\frac{\mu_t}{\sigma_e}\frac{\partial \varepsilon}{\partial x_i}\right) + c_1\frac{\varepsilon}{k}(P + G)(1 + c_{3\varepsilon}R_f) - c_2\rho\frac{\varepsilon^2}{k}, \quad i = 1,2,3 \quad (7)$$

where $\sigma_k = 1.0$ and $\sigma_\varepsilon = 1.3$ are the turbulent Prandtl numbers for the k and ε, respectively, and $c_1 = 1.44$, $c_2 = 1.92$ are model constants. $P$ is the turbulent shear production:

$$P = -\overline{\rho u_i' u_j'}\frac{\partial u_i}{\partial x_j} = \mu_t\left(\frac{\partial u_i}{\partial x_j} + \frac{\partial u_j}{\partial x_i}\right)\frac{\partial u_i}{\partial x_j}, \quad i,j = 1,2,3 \quad (8)$$

The term $G$ is the buoyant contribution to the production of turbulent kinetic energy. This term has been modeled according to Rodi (1980) as

$$G = -\beta g_i \overline{\rho u_i' T'} = \beta\frac{\mu_t}{\sigma_T} g_i \frac{\partial T}{\partial x_i}, \quad i = 1,2,3 \quad (9)$$

where $\beta = -(1/\rho)\,\partial\rho/\partial T$ is the volumetric expansion coefficient of the fluid, $R_f'$ is a modified flux Richardson number defined as $R_f' = -G/(P + G)$, and $c_{3\varepsilon} = 0.8$ is a model constant. The aforementioned definition of the $R_f'$ (which is different from the usual one $R_f = -G/P$) is after Rodi (1980) and is associated with the value of the constant $c_{3\varepsilon}$. The extra terms in the k-ε model to account for buoyancy effects have been previously tested in problems of stratified flows (Rodi 1980, Markatos *et al.* 1982), with a certain degree of success, thus extending the universality of the second-moment level of turbulence closure (Launder *et al.* 1984).

### Numerical solution of the equations

The governing equations just described are written in a generalized coordinate system in their strong conservation form and are solved numerically. A nonorthogonal coordinate transformation is made according to Glekas *et al.* (1987), and the physical space is transformed into a unit cube. The equations are integrated over the finite volume surrounding a grid point. Discretization is made using the hybrid scheme for the convection terms and a central difference scheme for the diffusion terms. After discretization, the equations are cast into the general finite difference form:

$$(A_P - S_P)\Phi_P = A_E\phi_E + A_W\Phi_W + A_N\Phi_W + A_S\Phi_S + A_D\Phi_D + A_U\Phi_U + S_u^\Phi \quad (10)$$

with $A_P = A_E + A_W + A_N + A_S + A_D + A_U$, $\phi: u_1, u_2, u_3, p, T$, k, ε, and $A_i^\phi$ coefficients linking the dependent variables on adjacent grid nodes.

The above set of equations are solved numerically by the alternating directional implicit method on a staggered grid, following the SIMPLE method of Patankar and Spalding (1972). Due to the strong stratification in the buoyant flows, stability problems arose. The use of small values (i.e., 0.1) of the underrelaxation factors during the first steps of the iterative procedure gave a solution to these problems. The model was run on a DEC-3100 workstation, and a run time of 40 hours was required for a typical case of the stably stratified 3-D flow field, as the one discussed in the section on stable cases for the 3-D axisymmetric hill.

### Boundary conditions

Since the flow field studied is elliptic, boundary conditions on all boundaries are necessary. In the inlet boundary the velocity distribution described in the experiments was used. For the top and lateral boundaries of the flow field Neumann boundary conditions were used usually, except for the main velocity component on the upper boundary, where a Dirichlet boundary condition was imposed. On the solid surfaces the no-slip boundary condition on the velocity was applied and the appropriate wall functions (Launder and Spalding 1974) were adopted. A summary of the boundary conditions used are shown in Table 1. Care must be taken when applying the wall functions, with the high Reynolds number version of the k-ε model, in satisfying the condition that $y^+ = \rho c_\mu^{0.25} k^{0.25} y_p/\mu$ be greater than 30, where $y_p$ is the distance of the first grid point from the wall. This was found necessary particularly in stably stratified flows; therefore, in the problems studied in this paper the first grid node was set in such a distance from the wall, so that everywhere in the flow domain the above condition was satisfied.

## Presentation and discussion of the results

Six different flow cases are discussed in this paper. Two of them concern the turbulent flow field past a 2-D fence under neutral and stable stratification. The other cases deal with the turbulent flow field around a 3-D hill for neutral and three different classes of stable stratification.

**Table 1** Boundary conditions

| Boundary | $u_1$ | $u_2$ | $u_3$ | k | $\varepsilon$ |
|---|---|---|---|---|---|
| Inlet | Experimental | $u_2 = 0$ | $u_3 = 0$ | Klebanoff's distribution | $k^{3/2}/l$ |
| Outlet | $\frac{\partial u_1}{\partial x_1} = 0$ | $\frac{\partial u_2}{\partial x_1} = 0$ | $\frac{\partial u_3}{\partial x_1} = 0$ | $\frac{\partial k}{\partial x_1} = 0$ | $\frac{\partial \varepsilon}{\partial x_1} = 0$ |
| Wall | Nonslip conditions coupled with wall functions | | | $\frac{\partial k}{\partial x_2} = 0$ | $\varepsilon_p = k^{3/2}/l_p$ |
| Upper | $u_1 = U_\infty$ | $\frac{\partial u_2}{\partial x_2} = 0$ | $\frac{\partial u_3}{\partial x_2} = 0$ | $\frac{\partial k}{\partial x_2} = 0$ | $\frac{\partial \varepsilon}{\partial x_2} = 0$ |
| Lateral | $\frac{\partial u_1}{\partial x_3} = 0$ | $\frac{\partial u_2}{\partial x_3} = 0$ | $\frac{\partial u_3}{\partial x_3} = 0$ | $\frac{\partial k}{\partial x_3} = 0$ | $\frac{\partial \varepsilon}{\partial x_3} = 0$ |

$l$, length scale; $p$, the nearest grid node to the wall

### *The two-dimensional fence*

Ogawa and Diosey (1980) conducted measurements in the region behind a 2-D fence of height $H = 0.04$ m, placed in a wind tunnel with the capability for simulating thermal stratification, using a two-color laser Doppler anemometer. The anemometer could measure the two velocity components simultaneously, and because of the frequency shift employed, reverse flow could also be measured. These experiments were chosen to be simulated in the present work because of their low experimental uncertainty and adequate information on the experimental boundary conditions for the neutral and stable cases. For the neutral flow the ambient air temperature $T_a$ was kept constant at $T_a = 18.5°C$ and the free stream velocity was $U = 1.99\ ms^{-1}$. A logarithmic oncoming velocity profile was created, and the fence was placed well within the boundary layer $\delta(H/\delta = 0.2)$. For the stable case (Ri = 0.23) the floor temperature was kept constant $T_f = 11.2°C$ and the heated ambient air had a temperature of $T_a = 80.4°C$ while the free stream velocity was set equal to $1.92\ ms^{-1}$. The above experimental arrangement was simulated numerically. A Cartesian grid of 97 × 40 was generated for the numerical solution. The computational domain was extended $9H$ ($H$, the fence height) upstream and $36H$ downstream of the fence. The fence thickness is assumed to be infinitesimal. Grid independence tests using 70 × 40 and 99 × 60 grid sizes for the neutral flow were conducted, without any significant effect on the results. Thus, a 97 × 40 grid was used for the two cases.

**The neutral case.** Figure 1a shows the predicted streamlines for the neutral flow over the fence. The upstream retardation of the flow as it approaches the fence, the upward deflection of the streamlines over the fence region, and the large cavity area behind the fence are qualitative characteristics well depicted by the numerical method. The length of the cavity region is found equal to $13.2H$ ($H$, the fence height) in good agreement with the experimentally measured $13H$. The choice of the outlet boundary far away from the fence (about three times the cavity length), the placement of the fence well within the boundary layer ($H/\delta = 0.2$, a value that, according to Castro and Fackrell (1978) ensures the independence of the cavity wake length from this parameter), and also the satisfactory distribution of the grid points along the main stream direction with a fine mesh (97 × 40) led to successful predictions. Benodekar *et al.* (1985), using a coarser grid of 49 × 47, were obliged to employ a bounded skew hybrid discretization scheme and to make corrections to the turbulence model in order to predict correctly the cavity length.

Figure 1b presents the comparison between predicted

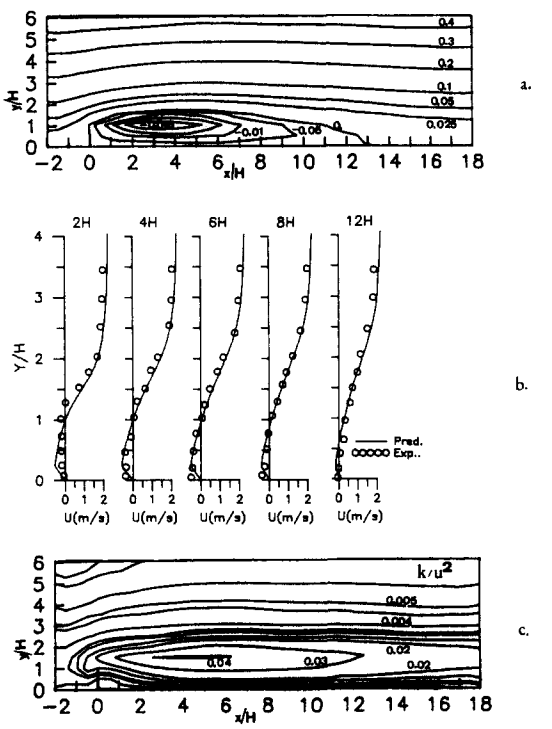


*Figure 1* Neutral flow field past the 2-D fence. (a) Streamlines; (b) velocity profiles; (c) turbulence intensity ($k/U\infty 2$) contours

streamwise velocity and the measured one within the cavity region. The predicted velocity field is in good agreement with the experiment; the height of the cavity is accurately predicted while differences are found in the velocities in the near wall layer. These differences are attributed to the coarseness of the numerical grid employed in this region (as can be seen by the linearity of the profile for the first numerical point used). The inability to use a fine mesh in the near wall region for this low Reynolds number problem stems from the need to apply wall functions and at the same time maintain a $y^+$ distance of 70 in order to get a reliable solution, in conjunction with the high Reynolds number version of the k-ε model. It should be noticed also that the experimental data have been compiled from the figures published by Ogawa and Diosey (1980), and, therefore, some inaccuracies are included in our plottings. In Figure 1c the turbulence intensity contours are presented, where it is seen that maxima exist along dividing streamline emanating from

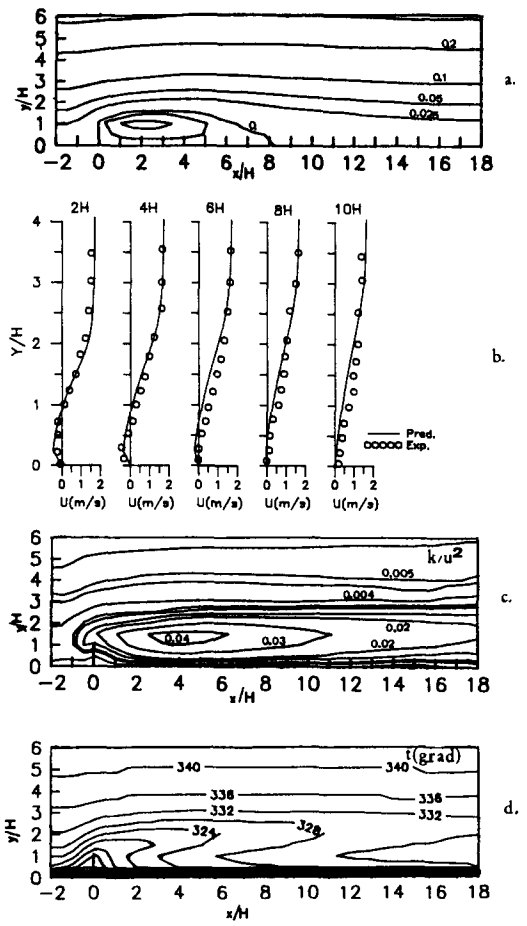


*Figure 2* Stable flow field past the 2-D fence. (a) Streamlines; (b) velocity profiles; (c) turbulence intensity ($k/U_\infty 2$); (d) temperature field

the top edge of the fence. The near wall levels of turbulence are very small to ensure a high turbulence Reynolds number.

**The stable case.** For the stable flow case (Ri = 0.23) the predicted streamlines are presented in Figure 2a. The reduction of the cavity length, compared with the neutral one, is a result of buoyant forces acting downward on the fluid. The upward displacement of the streamlines is slightly smaller than in the neutral flow field, indicating the damping effect of stability on the vertical direction. However, this damping is underestimated by the numerical method, as the measured velocity profiles, which are presented in Figure 2b, show. The predictions compare well with the experiment up to about $5H$ downstream of the fence; afterward the numerical method underestimates the velocity values near the wall and consequently overestimates the recirculation region length. The latter reveals an underestimation of the buoyancy effects. More specifically the results show a cavity wake length equal to $R_{Lstable} = 8.5H$ ($= 0.63R_{Lneutral}$), against the measured one, $R_{Lstable} = 7H$ ($= 0.54R_{Lneutral}$). This difference can be attributed to the coarse grid resolution near the wall region as discussed earlier and also to the inadequate buoyancy modeling in the two-equation turbulence closure as indicated also by Launder *et al.* (1984). Figure 2c presents the turbulence intensity contours for the stable case. The maximum of the turbulence intensity increases in value and extends in a greater area than in the neutral case. This happens due to the local unstable thermal stratification in this region of the shear layer, as can be seen in Figure 2d, where the distribution of the temperature field is presented. Outside this region turbulence levels are smaller than in the neutral case. In the area of separated shear layer, unstable thermal stratification is created, which increases the turbulence levels. On the contrary, the stable stratification, which prevails elsewhere in the flow field, causes a decrease of the turbulence intensity. The results seem to be realistic, although no experimental streamlines or temperature measurements are available for comparison.

### *The three-dimensional axisymmetric hill*

**The neutral case.** The experiment of Lawson (1984) around an axisymmetric hill placed in a wind tunnel was simulated for the neutral case. The experiment has been conducted in the EPA wind tunnel and a complete set of the measurements was reported. The model hill is described by the equation $h(r) = (h + c)/(1 + (r/L)^4) - c$, with $h = 15.45 \times 10^{-2}$ m as the maximum hill height, $L = 38.75 \times 10^{-2}$ m, and $c = 0.97 \times 10^{-2}$ m. The maximum terrain slope is about 24° so the hill is moderately steep, causing, as the experiments suggest, a flow separation in the lee side. The same model hill has been also used for the stratified flows experiments (Snyder *et al.* 1985) and therefore it was chosen for the numerical simulations in the present study.

A numerical grid of 35 × 31 × 25 size was generated (Figure 3a) for the numerical solution of the governing equations. The domain of integration was extended $25h$, $13h$, and $14h$ in the longitudinal, vertical, and crosswind directions, respectively, and the calculations started $5h$ upstream of the hill. The inlet conditions described by Lawson (1984) were imposed, while Klebanoff's data for a flat plate were used as inlet conditions for the turbulent kinetic energy. Figure 3b presents a vector plot of the flow field at about $0.045h$ and $0.15h$ above the hill surface. The flow separation in the lee side of the hill is clear and in good agreement with the experiments, where a small recirculation region was detected, using a dual Pitot tube (Lawson 1984), starting at a distance of $1.73h$ downwind of the hilltop and having a length of $1.95h$. In Figure 3c the predicted velocity profiles at several locations along the hill centerplane are presented. Good agreement with the experimental measurements is observed. A discrepancy in the near wall region within the recirculation area could be attributed to the experimental uncertainty. Figure 3d presents the comparison between the computed and the measured turbulence intensities along the vertical direction. The experimental values refer to the vertical component of the turbulence intensity ($\sqrt{u_2'^2}/u_{ref}$), while the computed ones refer to the total turbulence intensity ($k^{1/2}/u_{ref}$). For this reason the comparison should be made in a qualitative rather than a quantitative way. The quantitative agreement is satisfactory, but the computations underestimate the turbulence levels, especially downstream of the hilltop. This is possibly attributed to the inadequacy of the employed turbulence model to create high rates of diffusion transport of turbulent kinetic energy k upward in the vertical direction. Results were also obtained using a numerical grid of 19 × 20 × 10, and they are presented in Figure 4, where the dependence of the results on the coarse grid is obvious.

**The stable cases.** For the stable flow field study, the experiments of Snyder *et al.* (1985), conducted with an axisymmetric model hill in a towing tank, were simulated. The hill was the same as the one used in the neutral case, while the density stratification was achieved by means of a salinity gradient inside the towing tank. Three different Froude

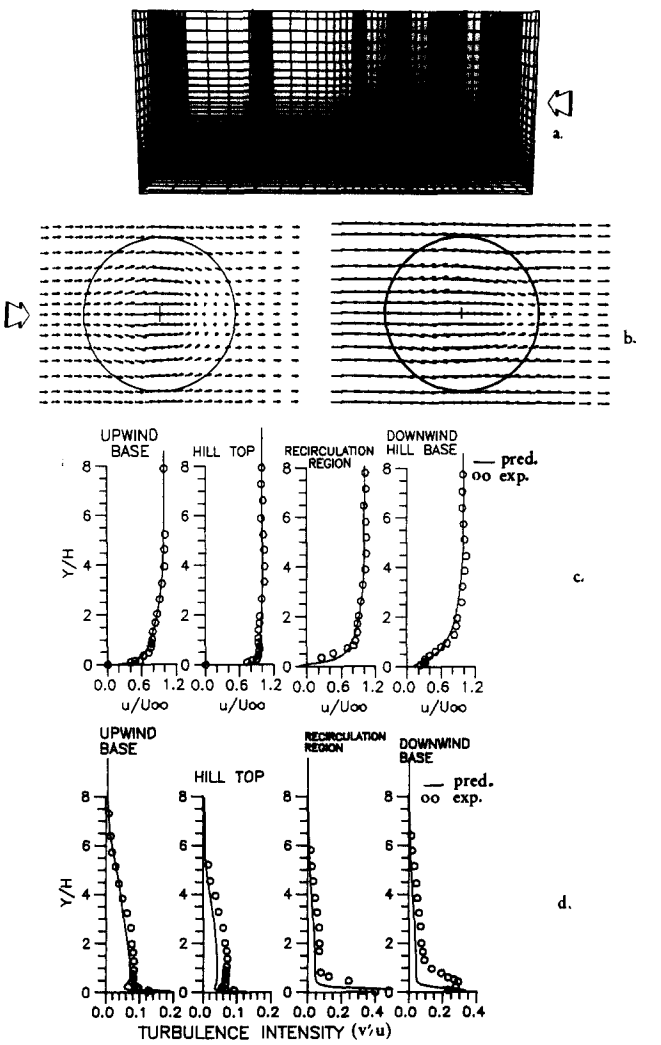


*Figure 3* Neutral flow field around the 3-D hill. (a) The numerical grid (only a few lines plotted); (b) vector plots at 0.045$h$ and 0.15$h$ above the hill surface; (c) velocity profiles; (d) turbulence intensity profiles

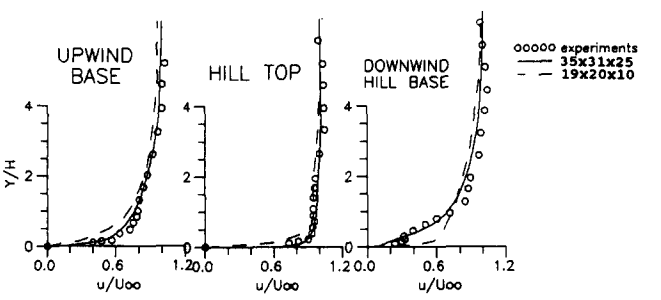


*Figure 4* Velocity profiles with various grid sizes

numbers, namely, Fr = 2, 1, and 0.6, were studied. The density gradient was kept constant during the experiments, and the towing speed $U_t$ was adjusted to obtain the desired Froude number $\mathrm{Fr} = U_t/(gh\,\Delta\rho/\rho)^{1/2}$, where $\Delta\rho$ is the density difference between the base and the top of the hill, $h$ is the hill height, and $g$ is the gravity acceleration. For the numerical approach a uniform inlet velocity profile was used. The towing speed $U_t$ was set equal to 0.33 $\mathrm{ms}^{-1}$, 0.167 $\mathrm{ms}^{-1}$, 0.1 $\mathrm{ms}^{-1}$ for Fr = 2, 1, and 0.6, respectively. The dimensions of the whole integration domain along the longitudinal, vertical, and crosswind directions were 24$h$, 8$h$, and 10$h$, respectively. A numerical grid of 40 × 12 × 19 was used for the three cases examined.

The Fr = 2 was the weaker stratification case studied. In Figure 5 the predicted flow field over the hill at 0.15$h$ above the hill surface is shown. The stratification is strong enough not only to suppress the boundary-layer separation observed in the lee side for the neutral case, but also to accelerate the flow substantially. As the uniform flow approaches the hill local retardation of the flow starts to appear both due to pressure effects and to boundary-layer formation, while the flow accelerates at the hill crest. Figure 6 presents a comparison of the streamline trajectories, as they are predicted by the numerical method, with the measured ones. The trajectories originate from various heights and also from different locations offset to the central plane. From the vertical displacements of the streamline trajectories in Figure 6a, the effect of the stable stratification becomes obvious in the lee side of the hill, where a serious, though less than that experimentally observed, downward displacement is noticed. The difference between the predicted and the experimental displacements can be attributed to the coarse grid resolution near the wall region and also to the underestimation of the buoyancy effects regarding the vertical motions damping, as discussed earlier. The predicted lateral deflections of the streamline trajectories, as presented in Figure 6b, are in good agreement with the experiments. The deviation from the symmetry plane is obvious; due to the stable stratification the fluid is forced to deviate essentially in the lateral direction.

In Figure 7a the vector plots of the flow field for Fr = 1 at 0.15$h$ above the hill surface are presented. Due to the stronger stratification a greater flow deceleration is observed on the lee side of the hill, while the acceleration at the hill crest is greater than in the Fr = 2 case. Figure 7b compares the predicted streamline trajectories for Fr = 1 with the experimental measurements and against the Fr = 2.0 flow field trajectories. The vertical downward displacement and the lateral deflection are more intense than in the previous case and compare well with the experimental observations. The strong deceleration of the flow in the lee side implies a trend toward separation, with increasing stability.

Separation on the lee side occurs in the Fr = 0.6 case, where the beginning of a hydraulic jump appears. A vector plot over the hill surface at 0.15$h$ from the wall is presented in Figure 8a. As the flow approaches the hill it decelerates strongly; reaching the hilltop the flow accelerates substantially because of the strong stable stratification, while proceeding to the lee side a lee wave dominated separation occurs. This separation

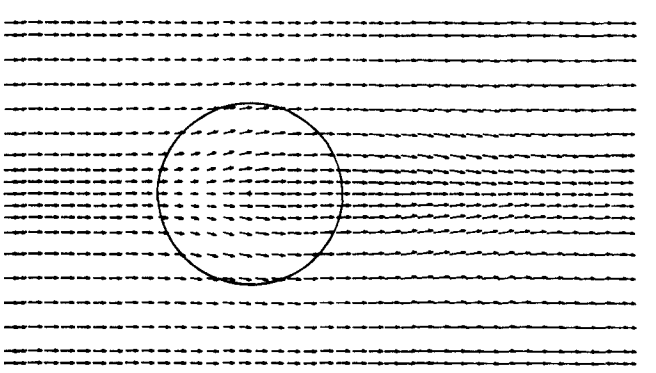

*Figure 5* Vector plot at 0.15$h$ above the hill surface for Fr = 2

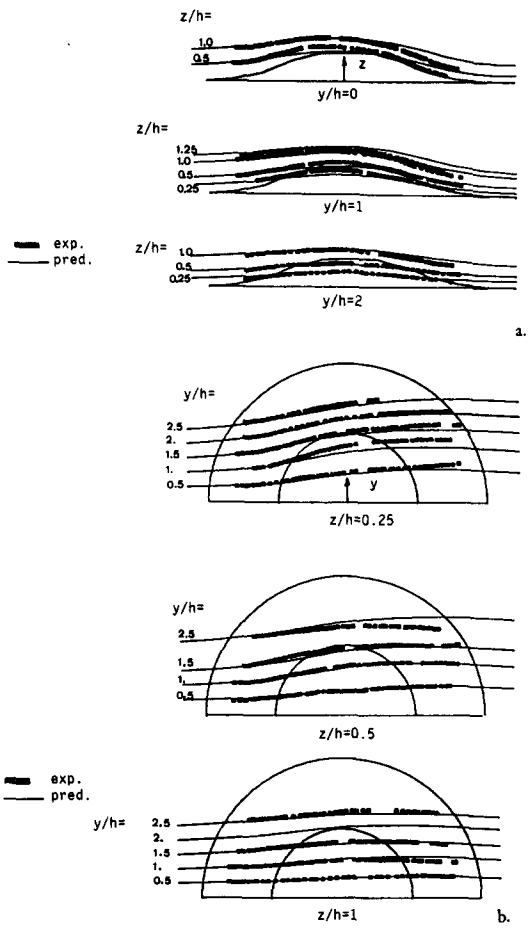


*Figure 6* Streamline trajectories over the 3-D hill for Fr = 2. (a) Vertical deflections; (b) lateral deflections

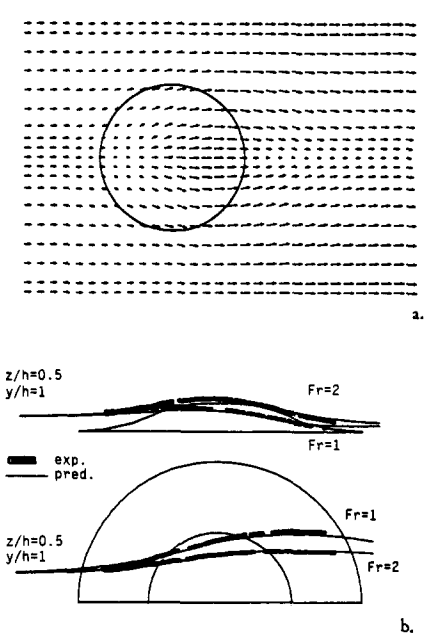


*Figure 7* Stable flow field (Fr = 1) over the 3-D hill. (a) Vertical plot at 0.15*h* above the hill surface; (b) streamline trajectories

is associated with a hydraulic jump as it can be seen in Figure 8b, where the streamline trajectories along the hill centerplane are presented. The streamlines are lifted just before the downwind base, due to the existence of a recirculation zone attached to that base. As the experiments showed the plume path in this area was not steady and also the presented measurements (Snyder *et al.* 1985) stop just before the downwind hill base, while in the other cases measurements are presented for further downstream locations. A strong hydraulic jump in the lee side of a polynomial hill with maximum slope of 45°, for Fr = 0.4, has been also observed by Hunt and Snyder (1980). The computed hydraulic jump in our case is less intense because of the smaller lee slope (24°). The separation begins at a downstream distance from the hill center $x_{sep} = 0.48$ m such that $x_{sep}/(\pi L) = 0.360$. Hunt and Snyder (1980) state that the separation point lies at such a downwind distance from the hill $x_{sep}$, that satisfies the relationship: $x_{sep}/(\pi L) < F_L(1 - F_L^2 L^2)/8D^2) < 0.8$, where $L$ is the half height of the hill, $F_L$ is the associated Froude number, and $D$ is the depth of the towing tank. In the Fr = 0.6 case studied, $L = 0.424$ m, $F_L = 0.365$, and $D = 1.2$ m, and thus the just written relationship is satisfied. Figure 8c presents the streamline trajectory originating from a height 0.5*h* above the hill surface at offset 1.0*h*. The agreement with the experiment is very good and encouraging for using the developed method, even at low Froude numbers.

In Figure 9 a comparison between the predicted velocity profiles and the measured ones over the hill center for Fr = 2 and Fr = 1 is presented. The experimental values were taken from Thompson *et al.* (1988) where the authors measured the velocities over the center of the hill in the towing tank using a propeller anemometer and a video camera. The scatter of their measurements is about 15–20 percent while the experimental uncertainty as they stated is up to 10 percent. For Fr = 2 the predicted profile is in very good agreement with the experiments. For Fr = 1, although the near surface overspeed

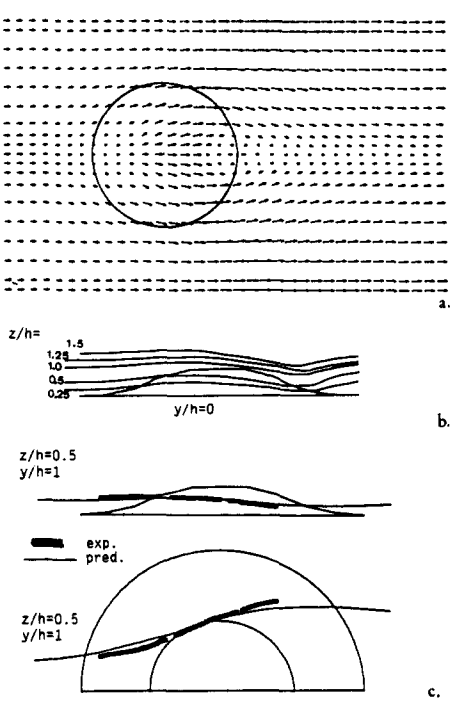


*Figure 8* Stable flow field (Fr = 0.6) over the 3-D hill. (a) Vector plot at 0.15*h* above the hill surface; (b) streamline trajectories along the centerplane; (c) streamline trajectory emanating from offset position

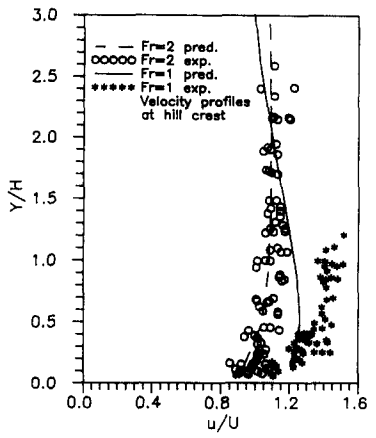


*Figure 9* Predicted and measured velocity profiles at the hill crest, for Fr = 2, Fr = 1

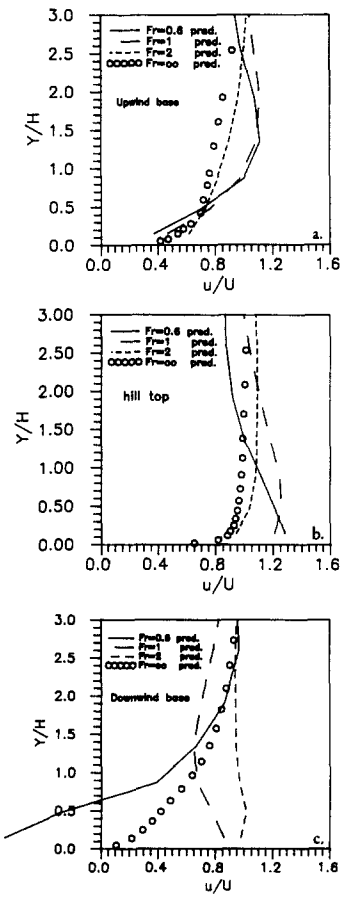


*Figure 10* Predicted velocity profiles along the centerplane of the 3-D hill, for various stability classes

is almost the same as the experimentally measured, a significant difference is observed higher. The computed values are about 14 percent smaller than the measured ones, which is within the experimental error. The overall agreement can be regarded as satisfactory since a great experimental uncertainty and an even greater scatter are involved in the measurements.

Figure 10 presents a comparison of the predicted velocity profiles at the upwind base, at the top, and at the downwind base of the hill for the neutral and the three stable flows studied. At the upwind base the velocity profiles for Fr = ∞ and for Fr = 2 are close to each other, and so are the Fr = 1 and Fr = 0.6 profiles. The flow deceleration is stronger for the less stable cases, especially those higher than 0.5*h* (*h*, the hill height). As the flow approaches the hill crest the gradual increase of the stratification has a straightforward impact on the shape of the profile, giving maximum overspeed near the hill surface for the lowest Froude number. Also for Froude numbers less than or equal to unity the fluid velocity decreases with height in contrast to the usually observed velocity increase for neutral and weakly stratified flows. Finally, in the downwind hill base the velocity for the neutral case has just started to recover after the small boundary-layer separation on the lee side of the hill. For Fr = 2 the velocity profile almost maintains its shape compared with the one over the hill crest. But for Fr = 1 the flow deceleration is substantial, while for Fr = 0.6 the lee wave dominated separation is present.

## Conclusions

A numerical method for solving stably stratified flows employing the time-averaged Reynolds equations was presented. The k-ε turbulence model was used, while the Boussinesq approximation for the density variations was adopted. The reliability and the accuracy of the method were established by comparing its predictions with the experimental measurements available for stable and neutral flow fields; good to very good agreement was found in most of the cases examined. Firstly, the neutral flow fields past a 2-D fence and a 3-D hill were simulated and then the stability effects on the flow development were studied with the developed method.

In the case of the 2-D fence the prediction of the neutral flow field was successful. The decrease of the cavity wake length due to buoyant forces in the stable case was satisfactorily predicted. The effects of buoyancy on the flow were clearly depicted by the developed method. A small underestimation of these effects was noticed, mainly due to the coarseness of the used numerical grid and possibly to inadequate turbulence modeling.

The successful predictions of the neutral flow past the 3-D hill established the reliability of the method for solving 3-D recirculating turbulent flows. The study of the stable flow over the 3-D hill showed that stable stratification forced a part of the fluid to bypass the hill laterally rather than overpass it, while the boundary-layer separation was completely suppressed. Also, the increase of the stability (i.e., decrease of the Froude number) gave rise to the lee wave dominated separation. The developed method gave reliable results over a broad range of stability classes (Fr = ∞, Fr = 2, Fr = 1, Fr = 0.06). Therefore, it can be safely used for studying stably stratified flows of engineering interest, i.e., pollutant dispersion over complex terrain.

## Acknowledgments

The authors acknowledge the collaboration of Dr. R. E. Lawson Jr. in supplying his experimental data. The first author acknowledges the financial support received by the Greek Scholarships Foundation.

## References

Benodekar, R. W., Goddard, A. J. H., Gosman, A. D. and Issa, R. I. 1985. Numerical prediction of turbulent flow over surface-mounted ribs. *AIIA J.* **23**, 359–366

Bergeles, G. and Athanassiadis, N. 1982. Numerical study of the flow around a surface mounted prism. *Proc. of Symposium on Refined Modelling of Flows*, Paris, France, vol. 1, 47–58

Brighton, P. W. M. 1978. Strongly stratified flow past three dimensional obstacles. *Q. J. R. Met. Soc.* **104**, 289–307

Castro, I. P. and Fackrell, J. E. 1978. A note on two-dimensional fence flows, with emphasis on wall constraint. *J. Int. Aerodyn.* **3**, 1–20

Castro, I. P., Snyder, W. H. and Marsh, G. L. 1983. Stratified flow over three-dimensional ridges. *J. Fluid Mech.* **135**, 261–282

Cebeci, T. 1974. Calculation of three dimensional boundary layers. I. Swept infinite cylinders and small cross flow. *AIAA J.* **12**, 779–786

Glekas, J., Bergeles, G. and Athanassiadis, N. 1987. Numerical solution of the transport equation for passive contaminants in three-dimensional complex terrain. *Int. J. Num. Meth. Fluids* **7**, 319–335

Haussling, H. J. 1977. Viscous flows of stably stratified fluids over barriers. *J. Atm. Sci.* **34**, 589–602

Hunt, J. C. R. 1980. Wind over hills. Review, American Meteorological Society Publ., pp. 107–144

Hunt, J. C. R. and Snyder, W. H. 1980. Experiments on stably and neutrally stratified flow over a model three dimensional hill. *J. Fluid. Mech.* **96**, 671–704

Ince, N. Z. and Launder, B. E. 1989. On the computation of buoyancy-driven turbulent flows in rectangular enclosures. *Int. J. Heat Fluid Flow* **10**, 110–117

Launder, B. E., Reynolds, W. C. and Rodi, W. 1984. *Turbulence Models and their Applications*. Editions Eyrolles, Paris, France

Launder, B. E. and Spalding, D. B. 1972. *Mathematical Models of Turbulence*. Pergamon Press, Oxford, UK

Launder, B. E. and Spalding, D. B. 1974. The numerical computation of turbulent flows. *Comp. Meth. Appl. Mech. Eng.* **3**, 269–289

Lawson, R. E., Jr. 1984. Effect of terrain-induced downwash on determination of good-engineering-practice stack height. U.S. Environmental Protection Agency, Research Triangle Park, NC, USA

Markatos, N. C., Malin, M. R. and Cox, G. 1982. Mathematical modelling of buoyancy-induced smoke flow in enclosures. *Int. J. Heat Mass Transfer* **25**, 63–75

Mouzakis, F. and Bergeles, G. 1991. Numerical prediction of turbulent flow over a two-dimensional ridge. *Int. J. Num. Methods Fluids* **12**, 287–296

Ogawa, Y. and Diosey, P. G. 1980. Surface roughness and thermal stratification effects on the flow behind a two dimensional fence. II. A wind tunnel study and similarity considerations. *Atmospheric Environment* **14**, 1309–1320

Patankar, S. V. and Spalding, D. B. 1972. A calculation procedure for heat, mass and momentum transfer in three-dimensional parabolic flows. *Int. J. Heat Mass Transfer* **15**, 1787–1805

Rodi, W. 1980. Turbulence models and their applications. In *Hydraulics. A State of the Art Review*, Int. Assoc. Hydraulic Research Publ.

Rowe, R. D., Benjamin, S. F., Chung, K. P., Havlena, J. J. and Lee, C. Z. 1981. Field studies of stable air flow over and around a ridge. *Atmospheric Environment* **16**, 643–653

Snyder, W. H., Thompson, R. S., Eskridge, R. E., Lawson, R. E., Castro, I. P., Lee, J. T., Hunt, J. C. R. and Ogawa, Y. 1985. The structure of strongly stratified flow over hills: dividing streamline concept. *J. Fluid Mech.* **152**, 249–288

Snyder, W. H., Thompson, R. S. and Shipman, M. S. 1985. Streamline trajectories in neutral and stratified flow over a three dimensional hill. U.S. Environmental Protection Agency, Research Triangle Park, NC, USA

Thompson, R. S., Shipman, M. S. and Rottman, J. W. 1988. Moderately stable flow over a three-dimensional hill; a comparison of linear theory with laboratory measurements. *Tellus*. submitted for publication

Trifonopoulos, D. A., Glekas, J. P. and Bergeles, G. C. 1989. Reliability of two numerical codes in predicting the wind field in complex terrain. *Wind Eng.* **13**, 324–337